Interfacial interactions between urea formaldehyde and cellulose nanofibrils (CNFs) of varying chemical composition and their impact on particle boards manufacture (PBs)

Maria C. Iglesias
Auburn University
Philip S. McMichael
Auburn University
Osei A. Asafu-Adjaye
Auburn University
Brian K. Via
Auburn University
Maria S. Peresin (msp0031@auburn.edu)
Auburn University https://orcid.org/0000-0003-2619-5320

Research Article

Keywords: cellulose nanofibrils, LCNF, urea formaldehyde, QCM-D, interfacial interactions, cellulosic nanofibers, wood adhesives

DOI: https://doi.org/10.21203/rs.3.rs-315097/v1

Abstract

Wood-based panels are commonly used as building materials for interior and exterior purposes. Their production and utilization have increased over the past decades due to the useful properties they present. Adhesive-bonded products make up to 80% of the wood alternatives on the global market, and of that, urea-formaldehyde (UF) makes up approximately 81% of the resins used. Formaldehyde-based resins are used due to their effectiveness and low cost, as well as their ease of application and lack of color. Nevertheless, their main disadvantages are the lack of tackiness and the emission of formaldehyde over time. To improve UF performance, the utilization of microfibrillated cellulose, has been demonstrated to be effective. However, more understanding on the mechanisms of the interactions is of relevant importance.

In this work, we studied interfacial interactions between UF with bleached (BCNF) and unbleached (LCNF) cellulose nanofibrils using Quartz Crystal Microbalance with dissipation monitoring (QCM-D) technique observing the superior performance of lignin-containing CNF. Additionally, the surface free energies were investigated using Contact Angle Measurements (CA) showing a decrease of the values mainly when utilizing LCNF, which was later correlated with the wettability properties of the particle boards (PBs). PBs with different adhesive/CNF formulations were produced showing larger improvements when adding LCNF in terms of modulus of elasticity (MOE), modulus of rupture (MOR), and internal bonding (IB).

To gain a better understanding on the interactions between CNF and UF, CNF was fully characterized in terms of morphology, chemical composition, charge density, as well as thermal and colloidal stability.

1. Introduction

Wood-based panels are commonly used as building materials both for interior and exterior purposes. Their production and utilization has been increasing over the past few decades due to the good and useful properties and the environmental benefits they present (Hansted et al. 2019). Among the wood-panel alternatives, particle board, fiber board, and oriented strand board (OSB) are some of the most frequently used (Ayrilmis et al. 2016; Hansted et al. 2019). Specifically, for particle boards manufacturing, three layers are normally formed where larger particles are used for the core layer, improving the mechanical properties. Thinner particles are used for the two outer layers in order to obtain a smooth surface (Hansted et al. 2019).

Adhesive-bonded products make up 80% of the wood products on the global market, and of that, Urea-Formaldehyde (UF) makes up more than 81% of the resins used (Lei et al. 2008).

It was reported by the Food and Agriculture Organization Corporate Statistical Database (FAOSTAT) that in 2019 United States produced 4,346,542 m^3 of particles boards, being the main producer in North America (FAOSTAT 2019).

Urea formaldehyde resin (UF) is a commonly used resin that holds together the particles and confers the required mechanical properties to the panel for its final application. Along with UF, other formaldehyde-based resins are primarily used due to the combination of their effectiveness and relatively low cost (Amini et al. 2017), as well as their ease of application and lack of color (Salari et al. 2013). One of the most important disadvantages of UF when used for interior particle board is that this adhesive is well known as a carcinogen and its use poses a human health issue during both wood composite manufacturing and use (Diop et al. 2017). The emission of formaldehyde is most often caused by unreacted formaldehyde trapped as a gas in the structure, as well as formaldehyde dissolving in water that enters the panel (Salari et al. 2013).

Despite the high toxicologic risks when using this adhesive, the global formaldehyde business is expected to reach 36.6 million tons at the end of 2026, due to the construction market being the biggest consumer of these resins (Transparency Market Research 2018).

Other than adjusting the urea to formaldehyde ratio, various fillers can be utilized to reduce the amount of resin needed. Common fillers must be insoluble in UF, these include cellulose, silica, talc, and chalk (Claub et al. 2011). Traditional fillers are made of larger particles, limiting mobility and making homogenization difficult (Dukarska and Czarnecki 2016). Thus, smaller particles, i.e. nano-sized, can induce effective properties such as improved mechanical strength and thermal resistance (Dukarska and Czarnecki 2016), as well as lower resin consumption, thus substantially reducing costs. (Lei et al. 2008). Among the nano particles used as filler for wood adhesives, nanoclay and nano-SiO_2 are some of the reported on the literature (Lei et al. 2010; Zahedsheijani et al. 2012; Salari et al. 2013; Dukarska and Czarnecki 2016).

As the most abundant natural polymer in the world (Klemm et al. 2005), and due to the continuous improvement of technology designed to isolate materials to the nanoscale, cellulose has been positioned to be used in a number of high-performance applications. When reducing its size into the nanoscale, cellulose fibers can be separated into small particles generally known as nanocellulose (Klemm et al. 2011; Moon et al. 2011; Lavoine et al. 2012). These nanoparticles can be obtained by different approaches; the most commonly used are chemical and mechanical treatments to obtain cellulose nanocrystals (CNC) and cellulose nanofibrils (CNF), respectively. In recent years, nanocellulose has been increasingly studied for its many intriguing properties and immense potential. On the side of wood composites research, micro and nano fibrillated cellulose have been recently investigated as a filler for wood adhesives in particle boards (Mahrdt et al. 2016; Hansted et al. 2019; Morais Júnior et al. 2020), OSB (Veigel et al. 2011, 2012), and plywood (Kawalerczyk et al. 2020). Veigel et al. (2011) studied the effect of the addition of CNF fibers into UF for wood beams. As a result, they determined that by adding 2 wt.% of CNF, the adhesive toughness increased up to 45 %. Following the same approach, Veigel et al. (2012) reported the effect of nanocellulose reinforced UF and melamine urea formaldehyde (MUF) adhesives for particle boards and OSB manufacture. They demonstrated that by adding 1 wt.% of CNF, the fracture energy and fracture toughness can be improved for both wood panels. In addition, Mahrdt et al. (2016) described the addition of microfibrillated cellulose (MFC) to UF for particle boards resulting in better mechanical performance. These results were determined to be due to the larger particle size when

adding MFC, improving the adhesive availability for bonding with other particles. Recently, Kawalerczyk et al. 2020, studied the effect of CNC addition on plywood panels to react with phenol formaldehyde (PF) resins. They found that 3 g of CNC to 100 g d.m. of resin, was the optimum ratio to help the effective transference of stress along the bond line and they observed the better mechanical properties f the panels at that ratio.

On the attempts to reduce the adhesive consumptions, some research groups have worked on the production of wood panels using nanocellulose as a complete replacement for commercial adhesives. Diop et al. (2017) demonstrated that using 20% unbleached CNF at 3 wt.% of consistency on fiber board panels improved the internal bonding and modulus of rupture when compared with 15 and 25 % CNF addition. Recently, Kojima et al. (2018) did similar work on particle boards, showing that the higher the amount of CNF added to the panel, the better the properties. As a negative aspect, when comparing particles boards made only with UF or (PF), they concluded that the properties of the board with 20wt.% CNF corresponded to those of the boards with 1 wt.% UF or PF.

Although several groups have studied the addition of CNF or MFC to wood panels showing how the properties can be improved, the actual interactions between UF and CNF, which may help to improve the final properties of the boards, are unknown.

The objective of this work was to demonstrate how UF resins and CNF from bleached and unbleached cellulose pulps interact in real time by using the Quartz Crystal Microbalance with Dissipation Monitoring (QCM-D).

2. Materials And Methods

2.1. Chemicals

Commercial urea formaldehyde (UF) containing 65 % solid content was provided by Hexion. Ammonium sulfate [$(NH_4)_2SO_4$] with a molecular weight of 132.14 g/mol was purchased from MilliporeSigma Lot: AM1256517 846, hydrochloric acid (HCl) was purchased from Macron® batch number: 0000162657, and sodium hydroxide (NaOH) (50 % w/w) from J.T. Baker Lot: 642022 CAS 3727-03. The water used was deionized and purified with a Thermo Scientific Barnstead Nanopure (18.2 MΩ cm).

For charge density measurements, cationic polymer Polydimethyl diallyl ammonium chloride (p-DADMAC) 0.001 N, sample number 920, and anionic polymer Polyvinyl sulfuric acid potassium salt (PVSK) 0.001 N, sample number 919, were purchased from BTG.

2.2. Cellulose pulps

For the purpose of this work, two never dried samples from softwood, bleached and unbleached, were used as raw material for nanocellulose production. Cellulose pulps were kindly provided by a US kraft mill.

2.3. *Cellulose nanofibrils (CNF) production*

Cellulose nanofibrils were produced at the Forest Products Development Center from Auburn University. For this purpose, celluloses pulps were washed using a HCl they reached pH = 3 and left for 30 min at that pH in order to eliminate possible metallic particles. Then, pulps were washed using DI water until a pH of 5 was reached. Afterwards, the pH was adjusted to 9 using NaOH and left for 30 min to convert the fibers into their sodium form (Elisabet Horvath et al. 2006). Finally, cellulose pulps were washed using DI until the conductivity of the filtrate reached < 5µS/cm.

Once the pulps were properly washed, a suspension at 2 wt.% of consistency was prepared. They were fibrillated until reaching the nanoscale using the Masuko Supermasscolloider (MKZA-10-15J) allowing the materials to defibrillate. After the mechanical process, a gel-like consistency was obtained. Sodium azide was incorporated into the samples to avoid the microorganisms growing. Samples were stored in the cold room at 5 ºC until further use.

2.4. *Characterization of CNF suspensions*

Zeta-potential and charge density

The colloidal stability of the suspensions was assessed by measuring charge density and zeta potential. pH was measured using a SympHony Benchtop Multi Parameter Meter B30PCI (VWR®) equipped with pH and conductivity electrodes. Measurements were repeated 15 times and averaged. Zeta potential was measured using an Anton Paar Litesizer 500 (Graz, Austria). Samples were diluted at 0.01 %wt. and sonicated for 2 min with a cold bath to avoid heating of the samples A Vibra Cell sonicator (Newtown, CA) was utilized with 20 KW and 20 % of amplitude. To promote a better dispersion of the colloidal suspension. Charge density of the fibers was measured following the method described in Iglesias et al. 2020. Both, zeta potential and charge density were measured six times at the pH of the suspensions 6.5. A statistical analysis ANOVA was performed and reported.

Thermal stability

The thermal behavior of the samples was measured by Thermogravimetric Analysis (TGA). Dry samples were tested on aluminum pans in a TGA-50 from Shimadzu (Kyoto, Japan). Samples were heated from room temperature to 600°C at a rate of 10°C/min under a nitrogen atmosphere and the data was processed with ta60 software, version 2.11 from Shimadzu. The sample size was approximately 15 mg for all CNF. Measurements were performed in duplicate.

Qualitative chemical composition

Chemical and structural composition of the samples was analyzed by Fourier-transform infrared spectroscopy with attenuated total reflectance accessory (FTIR-ATR) using a PerkinElmer Spotlight 400 FT-IR Imaging System (Massachusetts, US) with an ATR accessory. Before the measurements, a background spectrum was recorded for each unique sample. Afterwards, all spectra were collected from

400 to 4000 cm^{-1} with a 4 cm^{-1} wavenumber resolution after 64 continuous scans. The baseline was corrected, and the data was processed with Spectrum 6 Spectroscopy Software (PerkinElmer, Massachusetts, US). Measurements were performed by duplicate.

Morphology

The morphology of the samples was studied utilizing Atomic Force Microscopy (AFM). For AFM imaging, silicon surfaces were cleaned using UV ozone for 30 min and submerged for 15 min into 0.1 wt. % polyethylenimine (PEI), which was used as an anchoring solution. CNF suspensions were diluted at 0.2 wt.% and sonicated for 2 min using a Vibra Cell sonicator (Newtown, CA) with 20 KW and 20 % of amplitude to promote delamination and prevent their agglomeration, with a cold bath to avoid heating of the samples. Suspensions were deposited onto a silica surface by spin coating technique. Images were obtained in tapping mode using an Anton Paar TOSCATM 400 (Graz, Austria) with a silicon cantilever. Image size was 5 µm x 5 µm. Images were processed with Gwyddion software 2.49 (SourceForge).

Rheological behavior

Rheological properties of the cellulose nanofibrils were measured using a strain-controlled rotational rheometer (Physica MCR302, Anton Paar). Rheological measurements were performed on a 25 mm diameter parallel plate fixture geometry. The sample was loaded on the rheometer and allowed to equilibrate for 10 min before investigation of rheological properties. Tests were performed with a solvent trap of deionized water to prevent water loss due to extensive testing. A preliminary shear protocol was performed at a shear rate of 0.001 s^{-1} for 20 min to prevent structure change before measuring oscillatory dynamics. The dispersion microstructure was investigated with amplitude sweeps to determine the linear viscoelastic region (LVR) without severe structure deformation and frequency sweeps at 0.1 % strain within LVR to measure storage (G') and loss (G") moduli across a range of angular frequencies. Finally, flow curve to investigate structure deformation under shear across a range of shear rates were measured. Measurements were performed at a constant temperature of 25 ºC.

2.5. *Interactions between UF and cellulose nanofibrils*

Surface contact angle measurements (SCA)

Surface free energy was determined by contact angle measurements using a Dataphysics Instrument OCA50 optical goniometer with DDE/3 (Filderstadt, Germany). Measurements were performed using three liquids with different polarities, namely ethylene glycol, diiodomethane, and water. The dispense drop was 2 µl in volume, at a fast speed. Contact angle results were utilized for surface free energy calculations utilizing the acid-based model.

Quartz Crystal Microbalance with Dissipation Monitoring (QCM-D)

Interactions between UF, bleached and unbleached CNF were studied with a QSense Analyzer from Biolin Scientific (Västra Frölunda, Sweden). The basic principle of the QCM-D is the measurement of the

changes in frequency (Hz) of a piezoelectric sensor that has a base resonance of 5 MHz and has overtones of 15, 25, 35, 45, 55 and 75 MHz; changes in the frequency resonance are proportional to a change in mass on the sensor, as only the surface is interacting with a flow of matter, and those changes are likewise correlated to the mass adsorption on the sensors surface (Example 1991; KSV Instruments Ltd 2002; Voinova et al. 2002).

All measurements were performed at 25°C with a constant flow of 100 µL/min. Gold crystals were previously coated with the different types of nanocelluloses utilizing the same method explained in Sect. 2.4.4. Once the sensors were coated, in situ experiments were performed inside the QCM-D chambers.

In the particle board industry, a hardener is commonly used to improve the properties of the final product. For this purpose, ammonium sulfate [$(NH_4)_2SO_4$] is commonly mixed with water and the adhesive for an effective wood particle impregnation. In our study, we prepared a solution of adhesive and hardener and analyzed the interactions between this mixture and the different nanofibers. Only the changes of the third overtone are presented.

2.6. Particle boards production and characterization

Particles board (PB) manufacturing

Particle boards with 8.4% of adhesive loading, with respect to the total weight of the panel, were manufactured. Only 1% of UF was replaced using BCNF or LCNF, the two different types of nanocelluloses previously characterized. Additionally, 0.6% of wax and 3% of hardener were used based on the wood particles and the adhesive, respectively. The components conforming the liquid phase on the PBs production were mixed all together and then sprayed on the wood particles. The initial moisture content (MC) of the wood particles was 3% while at the end of the spraying process and before pressing, the MC was ~ 8.9 ± 0.6% for all the samples. The target density was 0.6 g/cm^3 in order to produce high density panels.

Wood particles were placed inside a concrete mixer and covered with a vinyl plastic to avoid losing material while mixing. Then, the liquid phase was sprayed using a spray gun while the wood particles were continuously rotated in the concrete mixer.

After the mixing process, wood panels were hand-formed using a mold with dimensions 40 cm x 40 cm on top of a metal sheet. After forming the wood mat, a second metal sheet was placed on top of the mat. Two metallic stoppers with 1.1 cm of thickness were used during the pressing at each side of the wood mat, maintaining the thickness of the panels constant. Finally, wood mat was pressed using a Wabash hydraulic press (model 50-24-2TM) for 3 min at 2.5 MPa and 200 ºC. Finally, wood panels were storage in a conditioning room at a temperature of 22.5 ºC and 55.2 % of relative humidity, until characterization.

For practical purposes, panels were denoted as (i) UF, for PB containing only UF, (ii) UF/BCNF for PB containing 1% of bleached CNF, and (iii) UF/LCNF for PB containing 1% of unbleached CNF.

PBs characterization

For water absorption (WA), thickness swelling (TS), modulus of elasticity (MOE) and modulus of rupture (MOR) samples of 30.5 cm of length and 8 cm on width were used.

WA and TS were measured following Standard ASTM D1037-12. Samples were pre-labeled in eight points which were equally spaced at the edge of each side and 2.5 cm from the edge to the center of the panel. Samples were fully submerged into tap water and properly secured using extra weight to keep them always underneath water. After 2 hours, the samples were removed, and the excess of water was drained. Additionally, a paper towel was used to carefully eliminate the remaining water on the surface of the panels. PBs were weighted and the thickness was measured in the same eight points as at the beginning.

WA was calculated using the weight of the panels before and after seeing submerged on water (Eq. 1). Regarding TS, it was calculated utilizing the thickness before and after the panels were introduced into the water (Eq. 2).

$$\%WA = \frac{Weight_{final} - Weight_{initial}}{Weight_{initial}} x\ 100 \qquad (1)$$

$$\%TS = \frac{thickness_{final} - thickness_{final}}{thickness_{final}} x\ 100 \qquad (2)$$

To measure the mechanical performance of the panels, a Zwick/Roell Z010 equipped with different heads was utilized to measure MOE, MOR, and internal bonding (IB). Samples with dimensions of 5 cm x 5 cm were utilized for IB measurements. Tests were performed by quadruplicate for MOE, MOR TS, and WA, and eight times for IB; the average and standard deviations were calculated and reported.

3. Results And Discussion

3.1. CNF characterization

Zeta-potential and charge density

Table 1 summarizes solid content, pH, zeta potential, and charge density of the two different CNFs. For samples containing lignin, the charge density value was larger than for the bleached CNF. This could be explained due to the presence of lignin, where more carboxylic and OH groups are present within the surface of the fibers (Crestini et al. 2017). Regarding zeta potential, BCNF present a slightly higher value than LCNF. Zeta potential is related not only to the solid particles but also to the liquid of the media, describing the charging behavior at the solid-liquid interface. Two main mechanisms affect the charge

between electrochemical double layer charge; (i) acid-based reactions between the liquid media and the functional groups present on the solid, and (ii) the absorption of water ions. Although sample containing lignin present higher number of functional groups, this excess can inhibit the complete dissociation of acid-based groups or their protonation, thus, reducing their zeta potential as we observed in Table 1. This inhibition occurs due to due to the repulsions between the functional charged groups on the surface of the fibers (Thomas Luxbacher 2014).

Table 1
Dry content, pH, Zeta potential, and charge density for bleached and unbleached CNFs.

Property	Unit	BCNF	LCNF
Dry Content	wt.%	2.0 ± 0.0	2.0 ± 0.1
pH		6.5 ± 0.0	6.5 ± 0.1
Z-Potential	mV	-30.3 ± 0.8	-27.1 ± 1.1
Charge density	μeq/g	258.9 ± 14.9	302.2 ± 15.0

The statistical analysis ANOVA (α = 0.05) reveals a significative difference between zeta potential and charge density of bleached and unbleached samples.

Thermogravimetric Analysis (TGA)

The thermal decomposition and the derivative of the CNFs are presented on Fig. 1. Similar behavior can be observed for both samples. T_{max} can be related with the velocity at which the sample decomposed, which can be observed as the maximum temperature value of the derivative (dm/dT). In this study, $T_{max\ (BCNF)}$ = 340.5 ºC and $T_{max\ (LCNF)}$ = 334.1 ºC. Additionally, T_{onset} of both samples was similar, being this the temperature at which the loss mass on the sample becomes more apparent (Nair and Yan 2015). $T_{onset\ (BCNF)}$ = 291.4 ºC and $T_{onset\ (LCNF)}$ = 293.5 ºC. These results are in agreement to the ones reported on the literature for samples containing different amount of lignin (Herrera et al. 2018; Iglesias et al. 2020). Observing the derivatives curves, LCNF shows a small jump at 270°C. It has been described on the literature that lignin has a broad range of decomposition temperature due to the presence of different groups on its structure (Yang et al. 2007; Brebu and Vasile 2010). Thus, this small peak may correspond to the presence of lignin.

Fourier-transform infrared spectroscopy with attenuated total reflectance accessory (ATR-FTIR)

Figure 2 shows the FT-IR spectra for BCNF and LCNF nanofibers in the range of 400–4000 cm^{-1}. The peak at 1029 cm^{-1} was utilized as parameter to normalize the spectra. Such a peak corresponds to the C-O stretching vibrations of lignin and polysaccharides (Huang et al. 2016) and showed a higher intensity for the bleached sample which could be attributed to better mobility of the C-O to the absence of lignin. As can be observed when comparing the graphs, both samples present a FT-IR spectrum that is very

similar, since no chemical treatment was used. Similar results are reported on the literature for samples with different lignin contents (Iglesias et al. 2020).

In the fingerprint region the main differences between the samples can be observed at 1160 cm-1 due to the C-O-C stretching of the pyranose ring, corresponding to the cellulose structure, showing a larger intensity for the BCNF samples. Additionally, at 1104 and 897 cm-1 there are stretching vibrations corresponding to C-OH and C-C, respectively (Yang et al. 2007).

Microscopy

The morphology of the fibers observed in Fig. 3 was measured by Atomic Force Microscopy (AFM). It can be observed that the defibrillation of the samples; in general, are long fibers with only a few nanometers present in the diameter dimension. Both samples present an entangled structure.

Rheology

Rheological measurements assessed the viscous behavior of the samples. Figure 4 shows the flow curves for each sample. At lower shear rates, LCNF containing lignin shows a viscosity almost four orders of magnitude larger than BCNF. This could be due to lignin's presence, which inhibits the movement of the fibers, and thus, its viscosity increase. At high shear rates, both samples show similar viscous behavior which may be due to the alignment of the fibers as the shear rate increases. Similar rheological behaviors have been reported in the literature for samples with different lignin contents (Iglesias et al. 2020). The reduction of the viscosity as the shear rate increase, is beneficial when spraying the samples into the wood particles during the PBs manufacturing process.

3.2. Interactions studies between UF and cellulose nanofibrils

Surface contact angle measurements (SCA)

Initially, the surface free energy of the UF and the two different nanocelluloses, BCNF and LCNF, was measured showing values of 43.4, 44.7, and 42.3 mN/m, respectively. In order to observe how the interaction between UF/BCNF and UF/LCNF affect the surface free energy, silicon surfaces were coated with layers of both components and measured. The obtained data showed that there is a decrease of the surface free energy when incorporating CNF to the UF. Surface free energy of UF/BCNF and UF/LCNF were 43.2 and 42.8 mN/m, respectively. Results in Table 2 were performed by duplicate and averaged.

From Table 2 we can observe how the addition of nanocellulose to the UF, decrease its surface free energy. LCNF shows a higher decrease of the surface free energy of the adhesive compared with the BCNF sample. This could be related to the hydrophobic characteristics of lignin (Solala I. et al. 2019) present on the LCNF sample.

Quartz Crystal Microbalance with Dissipation Monitoring (QCM-D)

Figures 5a) and b) show the interaction between BCNF and LCNF and a mixture of UF with hardener, respectively. We can observe in both graphs the irreversible mass absorption on the surface after rinsing the system with water.

BCNF and LCNF surfaces prepared by spin coating were first stabilized in Mili-Q water, allowing the surface to hydrate. Once the systems were stable, a solution of UF, hardener, and water was flowed through the equipment channels and an apparent decrease of the frequency was observed. To model the surfaces, Broadfit mathematical model was applied, and the mass absorbed onto the surface was calculated.

For BCNF, the change on frequency was Δf = -311.1 Hz which was converted to 5.6 $\mu g/cm^2$. Additionally, after rinsing with water, LCNF present a Δf = -332.2 Hz, meaning that 5.9 $\mu g/cm^2$ of mass remained irreversible absorbed on the surface of the sensor.

As we can observed LCNF showed a slightly higher interaction with the adhesive solution, compared with BCNF sample. By analyzing the chemical groups present on each type of fiber, LCNFs are composed of not only cellulose and hemicelluloses, but also lignin. It is well known that kraft lignin possesses on its structure OH, COOH, and epoxy groups (Crestini et al. 2017) which may help to have strong interactions with the amide, carbonyl and OH groups present on the UF resin (Akinterinwa et al. 2020).

3.3. PBs characterization

Mechanical and physical testing of PBs were measured by quadruplicated, and the results were averaged. As can be observed in Table 2, particleboard properties improved with the addition of 1% CNF. Mainly, the utilization of LCNF shows the best properties of the panels. TS and WA decrease after 2 and 24hs. This could be explained due to the hydrophobic nature of the lignin present on the LCNF fibers. Complementary with these results, we observed a decrease of the UF's surface free energy with the addition of LCNF, which could be related to a reduction of the sample's wettability as probed with WA and TS results.

Regarding the mechanical properties of the panels, MOE, and MOR, improved with the addition of LCNF in 18, 25%, respectively. In addition, IB also increased a 33%, when adding LCNF. As we observed on the QCM-D analysis, the interactions between the nanofibers and the adhesive mixture are favored due to the higher charge density and functional groups present on the lignin.

Table 2
Experimental data for mechanical and physical properties of PBs with CNFs addition.

	Thickness swelling		Water absorption		IB	MOE	MOR
	2 hours	24 hours	2 hours	24 hours			
PBs	%	%	%	%	N/mm^2	MPa	MPa
UF	37.4 ± 1.5	45.8 ± 1.4	72.9 ± 2.3	91.2 ± 2.4	0.3 ± 0.1	752.2 ± 75.0	4.1 ± 0.4
UF/BCNF	41.5 ± 1.5	47.0 ± 1.4	64.7 ± 2.3	86.0 ± 2.3	0.3 ± 0.0	842.2 ± 70.4	4.5 ± 0.4
UF/LCNF	33.6 ± 1.4	43.3 ± 1.3	46.5 ± 2.4	77.3 ± 2.3	0.4 ± 0.0	889.0 ± 73.8	5.1 ± 0.4

4. Conclusions

In this work we have extensively analyzed the interactions between UF and cellulose nanofibrils with different chemical composition. As a general effect, we observed an improvement of the properties of the wood panels by replacing 1% of UF with BCNF and LCNF. The better properties when adding nanocellulose can be attribute to the ability of the nanoparticles to transfer the stress trough the bond line, thus, enhancing the bonding between the wood particles.

The larger interactions at the interfaces between LCNF and UF obtained by QCM-D analysis were confirmed when measuring the properties of the final particle boards. Additionally, the larger reduction of the surface free energy when using lignin-containing CNF, was also observed in the wettability properties of the panels, increasing the hydrophobic character and allowing lower thickness swelling and water absorption after 2 and 24 hours. The improved performance of the PBs when using LCNF, could be also attributed to the higher charge density of this sample, which may allow better interactions between the adhesive, nanocellulose, and wood particles.

Declarations

Acknowledgements

This work was supported by the Wood-Based Composites Center, a National Science Foundation Industry/University Cooperative Research Center (Award 1624536-IIP). Additional support from the USDA National Institute of Food and Agriculture, Hatch program (ALA013-384 17003) and McIntire-Stennis program (1022526) and the School of Forestry and Wildlife Sciences at Auburn University's is much appreciated.

Declaration

Funding

This work was supported by the Wood-Based Composites Center, a National Science Foundation Industry/University Cooperative Research Center (Award 1624536-IIP). Additional support from the USDA National Institute of Food and Agriculture, Hatch program (ALA013-384 17003) and McIntire-Stennis program (1022526) and the School of Forestry and Wildlife Sciences at Auburn University's is much appreciated.

Conflicts of Interest

The authors declare no conflict of interest.

Availability of data and material

The data that support the findings of this study are available from the corresponding author, MSP, upon reasonable request.

Code availability

Not applicable

Ethical approval

Not applicable

References

1. Akinterinwa A, Ismaila A, Aliyu B (2020) Concise Chemistry of Urea Formaldehyde Resins and Formaldehyde Emission. Insights Chem Biochem 1–6. doi: 10.33552/ICBC.2020.01.000507
2. Amini E, Tajvidi M, Gardner DJ, Bousfield DW (2017) Utilization of cellulose nanofibrils as a binder for particleboard manufacture. BioResources 12:4093–4110. doi:10.15376/biores.12.2.4093-4110
3. Ayrilmis N, Lee YK, Kwon JH et al (2016) Formaldehyde emission and VOCs from LVLs produced with three grades of urea-formaldehyde resin modified with nanocellulose. Build Environ 97:82–87. doi:10.1016/j.buildenv.2015.12.009
4. Brebu M, Vasile C (2010) Thermal degradation of lignin—a review. Cellul Chem Technol 44:353–363
5. Claub S, Allenspach K, Gabriel J, Niemz P (2011) Improving the thermal stability of one-component polyurethane adhesives by adding filler material. Wood Sci Technol 45:383–388. doi:10.1007/s00226-010-0321-y
6. Crestini C, Lange H, Sette M, Argyropoulos DS (2017) On the structure of softwood kraft lignin. Green Chem 19:4104. doi:10.1039/c7gc01812f
7. Diop CIK, Tajvidi M, Bilodeau MA et al (2017) Evaluation of the incorporation of lignocellulose nanofibrils as sustainable adhesive replacement in medium density fiberboards. Ind Crops Prod 24:3037–3050. doi:10.1016/j.indcrop.2017.08.004

8. Dukarska D, Czarnecki R (2016) Fumed silica as a filler for MUPF resin in the process of manufacturing water-resistant plywood. Eur J Wood Wood Prod 74:5–14. doi:10.1007/s00107-015-0955-4
9. Example A (1991) Dissipative QCM. Langmuir 1–3
10. FAOSTAT (2019) http://www.fao.org/faostat/en/#data/FO
11. Hansted FA, Hansted AL, Durango Padilla ER et al (2019) The use of nanocellulose in the production of medium density Particleboard panels and the modification of its physical properties. BioResource 14:5071–5079. doi:10.15376/biores.14.3.5071-5079
12. Herrera M, Thitiwutthisakul K, Yang X et al (2018) Preparation and evaluation of high-lignin content cellulose nanofibrils from eucalyptus pulp. Cellulose 25:3121–3133. doi:10.1007/s10570-018-1764-9
13. Horvath AE, Lindström T, Laine J (2006) On the indirect polyelectrolyte titration of cellulosic fibers. Conditions for charge stoichiometry and comparison with ESCA. Langmuir 22:824–830. doi:10.1021/la052217i
14. Huang Y, Wang Z, Wang L et al (2016) Analysis of lignin aromatic structure in wood fractions based on IR spectroscopy. J Wood Chem Technol 36:377–382. doi:10.1080/02773813.2016.1179325
15. Iglesias MC, Shivyari N, Norris A et al (2020) The effect of residual lignin on the rheological properties of cellulose nanofibril suspensions. J Wood Chem Technol 40:370–381. doi:10.1080/02773813.2020.1828472
16. Kawalerczyk J, Dziurka D, Mirski R et al (2020) The effect of nanocellulose addition to phenol-formaldehyde adhesive in water-resistant plywood manufacturing. BioResources 15:5388–5401. doi:10.15376/biores.15.3.5388-5401
17. Klemm D, Heublein B, Fink HP, Bohn A (2005) Cellulose: Fascinating biopolymer and sustainable raw material. Angew Chemie - Int Ed 44:3358–3393. doi:10.1002/anie.200460587
18. Klemm D, Kramer F, Moritz S et al (2011) Nanocelluloses: A new family of nature-based materials. Angew Chemie - Int Ed 50:5438–5466. doi:10.1002/anie.201001273
19. Kojima Y, Kato N, Ota K et al (2018) Cellulose Nanofiber as a Complete Natural Binder for Particleboard. For Prod J 68:203–210. doi:10.13073/FPJ-D-18-00034
20. KSV Instruments Ltd (2002) What Is a Quartz Crystal Microbalance – Qcm. 1–10
21. Lavoine N, Desloges I, Dufresne A, Bras J (2012) Microfibrillated cellulose - Its barrier properties and applications in cellulosic materials: A review. Carbohydr Polym 90:735–764. doi:10.1016/j.carbpol.2012.05.026
22. Lei H, Du G, Pizzi A et al (2010) Influence of nanoclay on phenol-formaldehyde and phenol-urea-formaldehyde resins for wood adhesives. J Adhes Sci Technol 24:1567–1576. doi:10.1163/016942410X500945
23. Lei H, Du G, Pizzi A, Celzard A (2008) Influence of nanoclay on urea-formaldehyde resins for wood adhesives and its model. J Appl Polym Sci 109:2442–2451. doi:10.1002/app.28359

24. Mahrdt E, Pinkl S, Schmidberger C et al (2016) Effect of addition of microfibrillated cellulose to urea-formaldehyde on selected adhesive characteristics and distribution in particle board. Cellulose 23:571–580. doi:10.1007/s10570-015-0818-5
25. Moon RJ, Martini A, Nairn J et al (2011) Cellulose nanomaterials review: structure, properties and nanocomposites. Chem Soc Rev Chem Soc Rev 40:3941–3994. doi:10.1039/c0cs00108b
26. Morais Júnior RR, Cardoso GV, Ferreira ES, Costa HL (2020) Surface characterization, mechanical and abrasion resistance of nanocellulose-reinforced wood panels. Surf Topogr Metrol Prop 8:025011. doi:10.1088/2051-672X/ab8aa5
27. Nair SS, Yan N (2015) Effect of high residual lignin on the thermal stability of nanofibrils and its enhanced mechanical performance in aqueous environments. Cellulose 22:3137–3150. doi:10.1007/s10570-015-0737-5
28. Salari A, Tabarsa T, Khazaeian A, Saraeian A (2013) Improving some of applied properties of oriented strand board (OSB) made from underutilized low quality paulownia (Paulownia fortunie) wood employing nano-SiO_2. Ind Crops Prod 42:1–9. doi:10.1016/j.indcrop.2012.05.010
29. Solala I, Iglesias MC, Peresin MS (2019) On the potential of lignin-containing cellulose nanofibrils (LCNF): a review on properties and applications. Cellulose 27:1853–1877. doi:10.1007/s10570-019-02899-8)
30. Thomas Luxbacher (2014) The ZETA guide - Principles of the streaming potential technique, First. Anton Paar GmbH., Graz, Autria
31. Transparency Market Research (2018) https://www.globenewswire.com/news-release/2018/01/03/1281428/0/en/Global-Formaldehyde-Market-is-expected-to-reach-36-6-million-tons-towards-the-end-of-2026-Transparency-Market-Research.html
32. Veigel S, Müller U, Keckes J et al (2011) Cellulose nanofibrils as filler for adhesives: Effect on specific fracture energy of solid wood-adhesive bonds. Cellulose 18:1227–1237. doi:10.1007/s10570-011-9576-1
33. Veigel S, Rathke J, Weigl M, Gindl-Altmutter W (2012) Particle board and oriented strand board prepared with nanocellulose- reinforced adhesive. J Nanomater 2012:1–8. doi:10.1155/2012/158503
34. Voinova MV, Jonson M, Kasemo B (2002) “Missing mass” effect in biosensor’s QCM applications. Biosens Bioelectron 17:835–841. doi:10.1016/S0956-5663(02)00050-7
35. Yang H, Yan R, Chen H et al (2007) Characteristics of hemicellulose, cellulose and lignin pyrolysis. Fuel 86:1781–1788. doi:10.1016/j.fuel.2006.12.013
36. Zahedsheijani R, Faezipour M, Tarmian A et al (2012) The effect of Na^+ montmorillonite (NaMMT) nanoclay on thermal properties of medium density fiberboard (MDF). Eur J Wood Wood Prod 70:565–571. doi:10.1007/s00107-011-0583-6

Figures

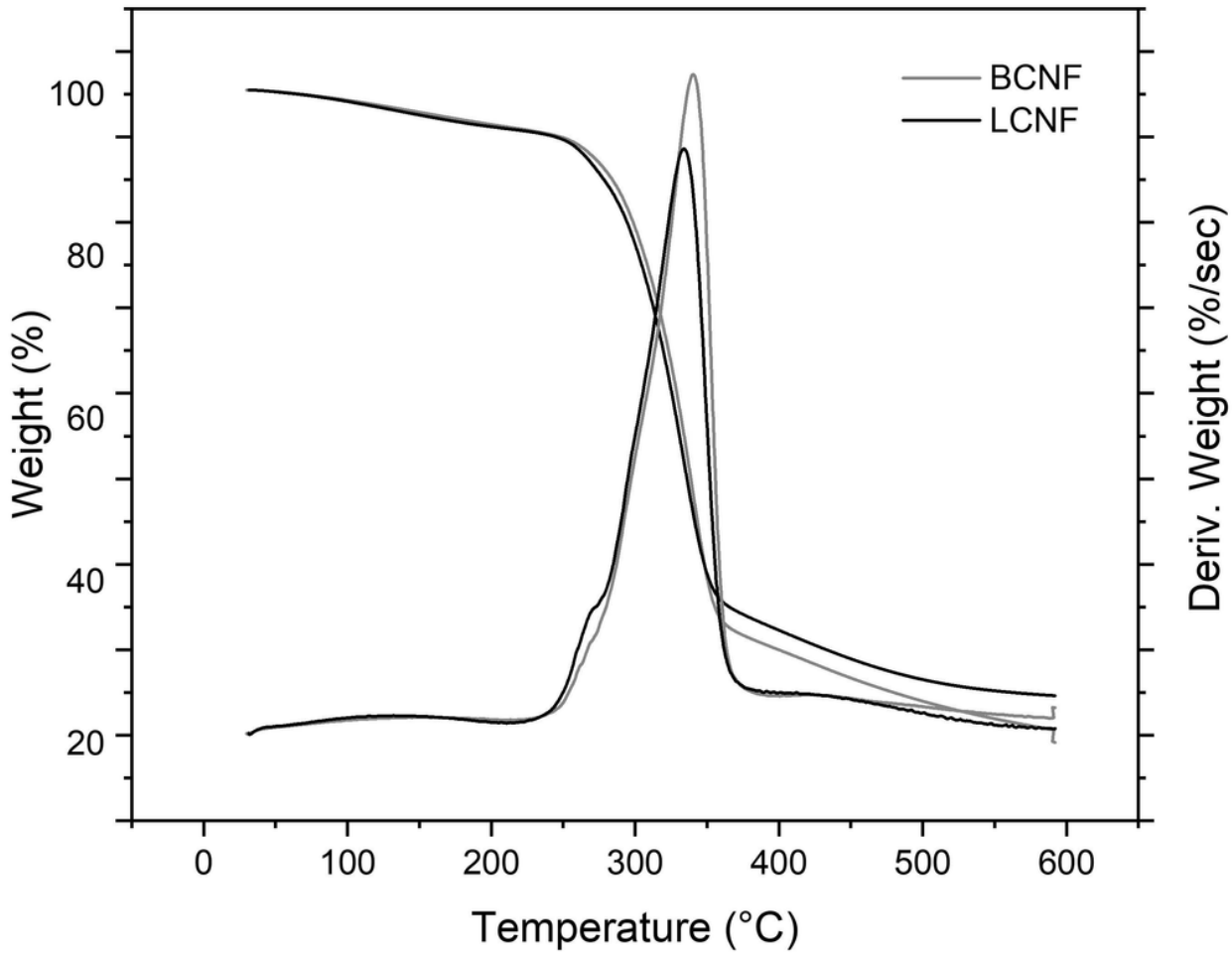

Figure 1

TGA spectra and weight derivative on BCNF (grey) and LCNF (black) measured in nitrogen atmosphere.

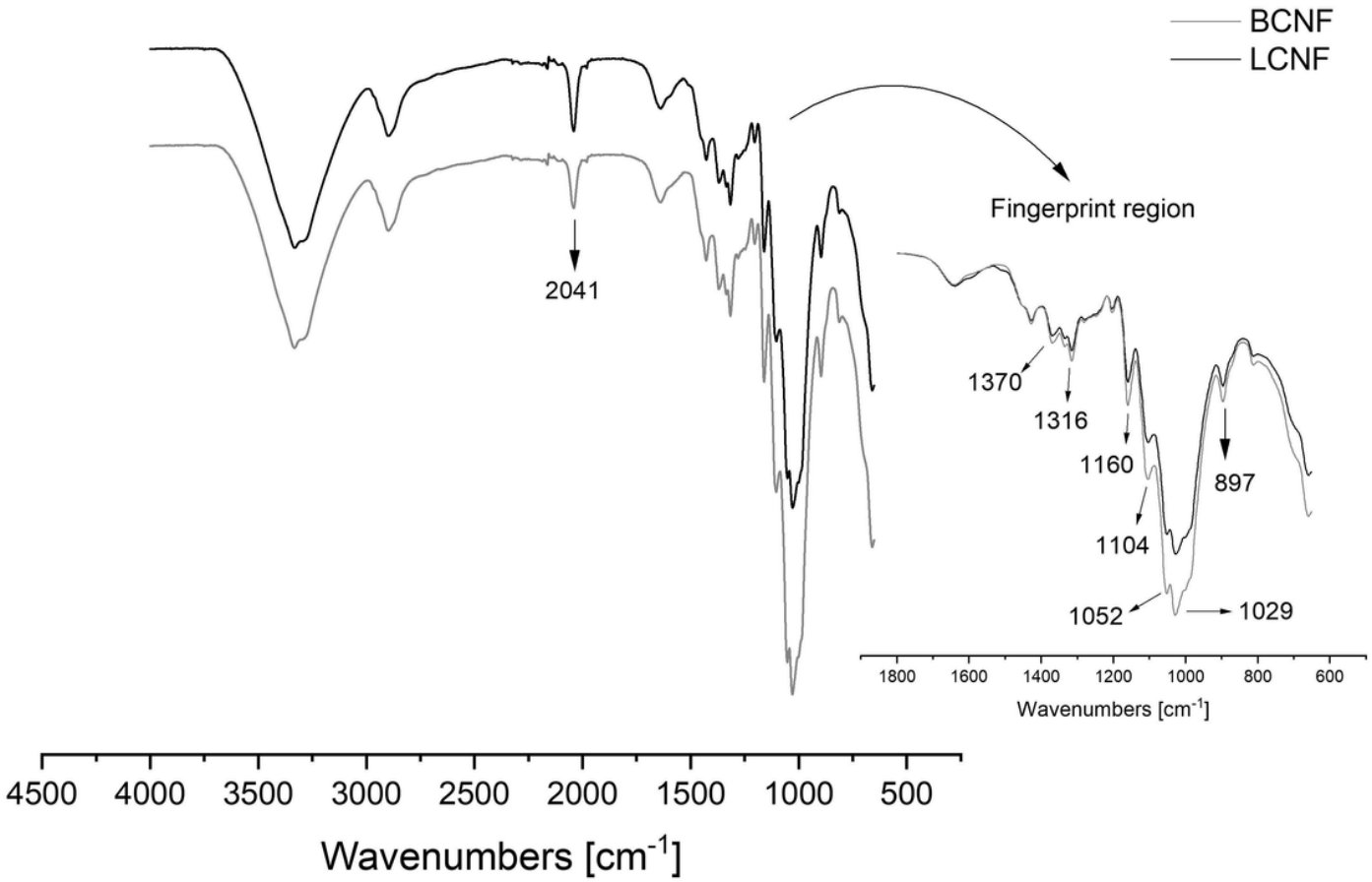

Figure 2

FT-IR spectra for BCNF (grey) and LCNF (black).

Figure 3

AFM topography images of a) BCNF and b) LCNF.

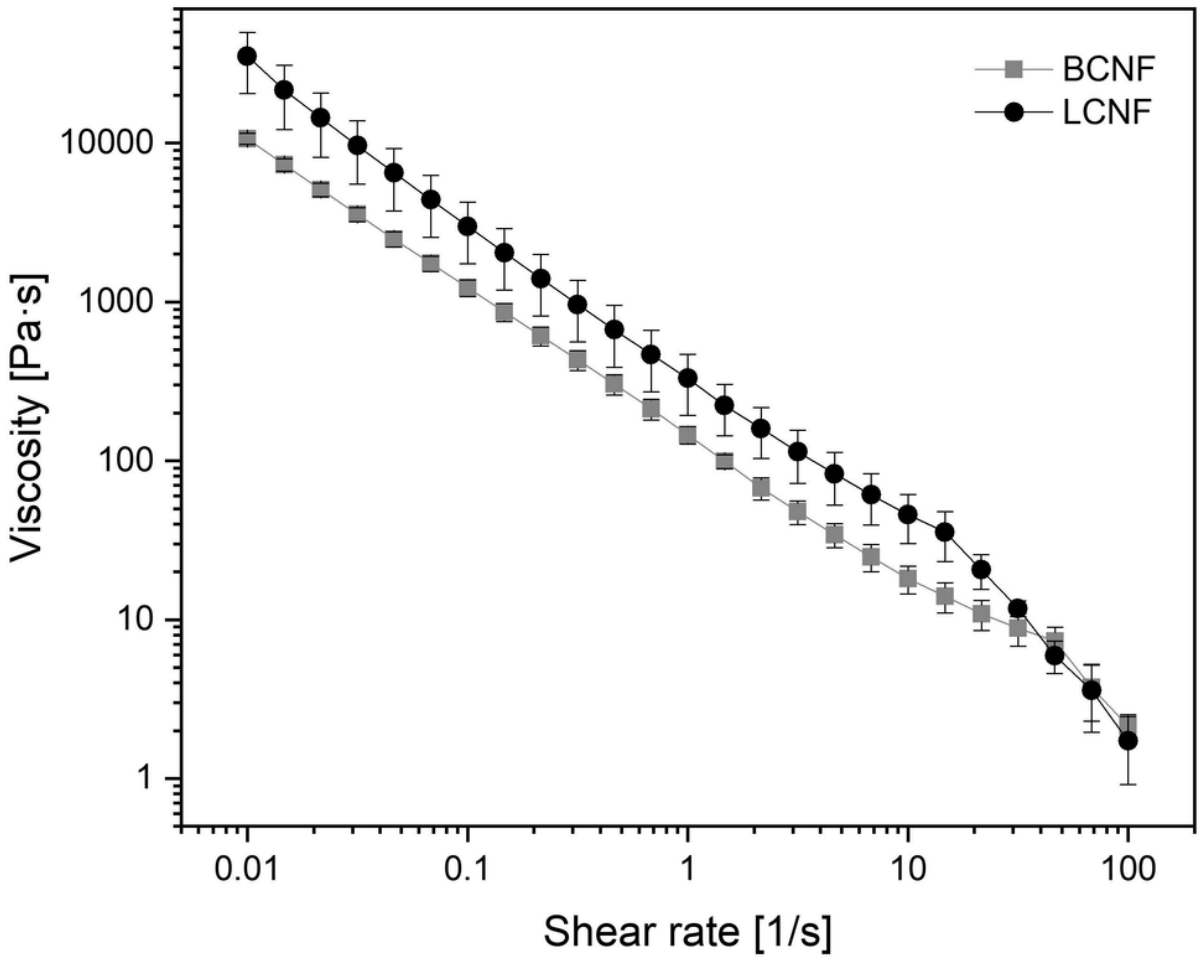

Figure 4

Flow curve of BCNF (grey square), and LCNF (black circles).

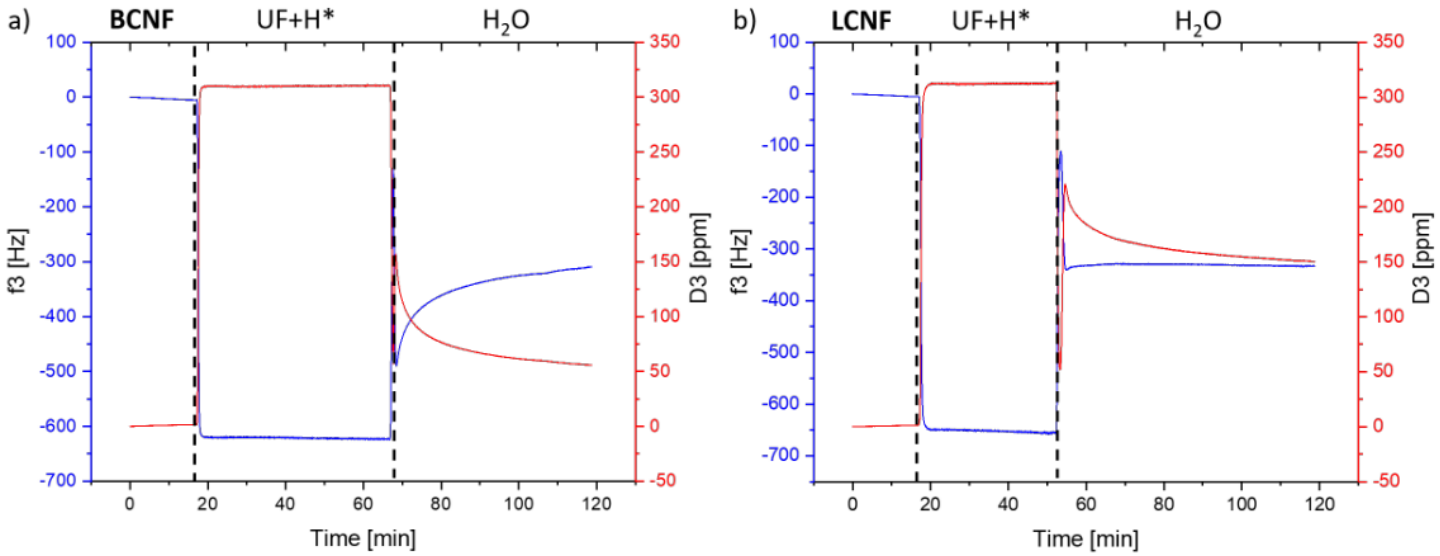

Figure 5

QCM-D spectra interactions between model surfaces of a) BCNF and b) LCNF, with a mixture of UF and hardener (UF+H*) both irreversible absorbed after rinsing with Mili-Q water.